Curvature Tuning: Provable Training-free Model Steering From a Single Parameter

Levang Hu*

Department of Computer Science Brown University leyang_hu@brown.edu

Matteo Gamba*

KTH Royal Institute of Technology mgamba@kth.se

Randall Balestriero

Department of Computer Science Brown University randall_balestriero@brown.edu

Abstract

The scaling of model and data sizes has reshaped the AI landscape, establishing finetuning pretrained models as the standard paradigm for solving downstream tasks. However, dominant finetuning methods typically rely on weight adaptation, often lack interpretability, and depend on heuristically chosen hyperparameters. In this paper, we take a different perspective and shift the focus from weights to activation functions, viewing them through the lens of spline operators. We propose Curvature Tuning (CT), an interpretable and principled steering method that modulates a model's decision boundary by injecting a single hyperparameter into its activation functions. We show that CT provably adjusts model decision boundary curvature and, more fundamentally, projects a model onto a space of smooth functions—thereby complementing current finetuning methods, whose effect lies primarily in feature adaptation. Making this hyperparameter trainable gives rise to a novel and highly parameter-efficient finetuning method. Empirically, CT improves both generalization and robustness. For example, it boosts downstream accuracy of ResNet-50/152 by 7.14%/8.46% over linear probing and 4.64%/1.70% over LoRA across 12 datasets, and improves robust accuracy on the ℓ_{∞} benchmark from RobustBench by 1032.64%/1494.46%. Our code is available at https://github.com/Leon-Leyang/curvature-tuning.

1 Introduction

The scaling of model and data sizes has given rise to foundation models, such as Llama3 [1] for natural language processing (NLP), DINOv2 [2] for computer vision (CV), CLIP [3]and SigLIP [4] for multimodal tasks, and OpenVLA [5] for embodied agents. These models have shown remarkable capabilities, accelerating a paradigm shift in artificial intelligence: transitioning from training task-specific models from scratch to leveraging models pretrained on large datasets and finetuning them for downstream applications.

Full finetuning, the process of steering¹ a pretrained model by adapting all its parameters to down-stream datasets, was once the primary approach for transferring knowledge. While it effectively

^{*}These authors contributed equally to this work.

¹In this paper, we use *steering* as a general term for tuning a model, including both training-based and non-training-based methods. We use *finetuning* to refer specifically to steering methods that adapt the model's parameters via training.

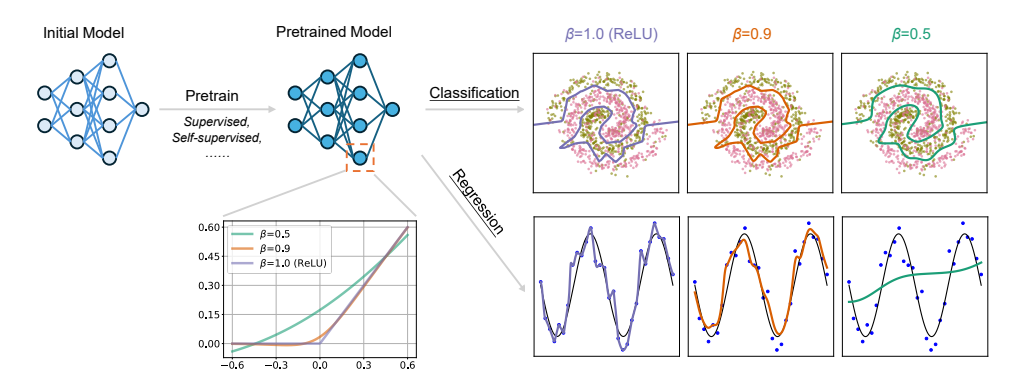


Figure 1: Illustration of Curvature Tuning (CT) on classification (top) and regression (bottom) tasks. The pretrained model for classification is a 3-layer MLP with hidden width 20 trained for 2000 steps; for regression, it is a 9-layer MLP with hidden width 64 trained for 20000 steps. **CT steers a pretrained model by replacing ReLUs with a** β -parameterized activation function and tuning β from 1 to 0, effectively modulating the model's decision boundary curvature.

enhances generalization [6] and robustness [7], it is computationally expensive at large model scales. To mitigate this, parameter-efficient finetuning (PEFT) methods such as Serial Adapter [8] and LoRA [9] have been introduced, which finetune only a small subset of parameters. However, these approaches usually lack interpretability and principled design. For instance, they treat the model as a black box, making it unclear how the model is steered for downstream tasks. Consequently they usually rely on heuristic choices—such as LoRA's rank, placement, and initialization—with minimal theoretical guidance. This leads to a natural question: how can we construct principled steering solutions addressing both efficiency and interpretability?

In this work, we answer the question by introducing a novel model steering perspective. We observe that despite differences in specific forms, existing finetuning methods all share a focus on adapting model weights—either by introducing new ones or updating existing ones. However, one critical component of the model has been largely overlooked: the activation functions (e.g., ReLU), which are responsible for the model's nonlinearity and, ultimately, its expressivity [10, 11].

Grounded in the spline interpretation of deep networks [12, 13], we propose **Curvature Tuning** (**CT**), a steering method that provably modulates a model's decision boundary curvature by injecting a single hyperparameter β into the activation function, as shown in Fig. 1. Additionally, allowing β to be trained leads to a novel finetuning method. We highlight four key advantages of CT below:

CT is more interpretable and principled. We show that CT provably modulates the curvature of the model's decision boundary with as few as only one hyperparameter.

CT complements current finetuning methods. More essentially, while current finetuning methods adapt features, CT projects the model to a space of smooth functions.

CT is highly parameter-efficient. As a steering method, *CT* introduces only one (hyper)parameter per network. As a finetuning method, *Trainable CT* still uses significantly fewer parameters than LoRA with rank one, requiring only 0.58% to 59.05% of the parameters used by LoRA in our experiments.

CT improves both generalization and robustness. For example, $Trainable\ CT$ boosts transfer accuracy of ResNet-50/152 by 7.14%/8.46% over linear probing and 4.64%/1.70% over LoRA with rank one across 12 downstream datasets. CT improves robust accuracy of ResNet-50/152 by 1032.64%/1494.46% on the ℓ_{∞} benchmark from RobustBench.

In summary, our key contributions are both theoretical and empirical. **Theoretically**, we propose Curvature Tuning (CT) and show that it provably modulates the model's decision boundary curvature, by projecting the model onto a space of smooth functions. **Empirically**, we introduce *CT* as a steering method and *Trainable CT* as a finetuning method, demonstrating improved generalization across five models and 12 downstream datasets, as well as robustness gains on the RobustBench benchmark [14].

The remainder of this paper is organized as follows: Section 2 reviews current finetuning techniques and introduces relevant spline concepts, the foundation for our method. Section 3 details our proposed method and its theoretical guarantees. Section 4 presents experimental results, and Section 5 summarizes our findings and potential future directions.

2 Background

This section first reviews current finetuning techniques and their limitations (Section 2.1), then introduces spline theory and its connections to deep networks as the foundation for CT (Section 2.2).

2.1 Current finetuning techniques and limitations

Finetuning refers to steering a pretrained model to improve its performance on downstream tasks through training. Initially, the common practice was to continue training all model parameters—a process known as *full finetuning*. Notable examples include GPT [6] and DINO [15]. However, as model sizes have grown, full finetuning has become increasingly costly and impractical, especially given the limited size of many downstream datasets. Given these challenges, *parameter-efficient finetuning (PEFT)* methods were developed to mitigate the cost while maintaining effectiveness.

We follow the categorization of Han et al. [16], which groups PEFT methods into four main categories. **Additive PEFT** introduces additional trainable parameters to the pretrained model, training only these new parameters during finetuning. Examples include Serial Adapter [8], Prefix-tuning [17], (IA)³ [18] and RoAd [19]. **Selective PEFT** identifies a subset of existing parameters for finetuning, with examples such as U-Diff pruning and S-Diff pruning [20]. **Reparameterized PEFT** decomposes pretrained weights into low-rank matrices, finetuning only the low-rank components, which are converted back during inference; examples include LoRA [9] and DyLoRA [21]. **Hybrid PEFT** combines multiple PEFT approaches, such as UniPELT [22] and S4 [23].

While PEFT methods differ in the parameters they update, they all adapt model weights and operate on learned features—an approach that often relies on heuristic tuning. For example, LoRA requires decisions about adapter placement [24], rank [21, 25], scaling [26], and initialization [27]. In contrast, as described in Section 3, CT introduces only a single hyperparameter into the activation functions that provably modulates the decision boundary curvature, offering a more interpretable alternative that instead operates on the model's underlying function space without changing model weights.

2.2 The spline formulation of deep networks

In this subsection, we review relevant concepts in splines, which provide a mathematical framework for understanding the relationship between piecewise-affine functions and deep networks (DNs).

A *spline function* is a continuous function $s:\mathbb{R}^D\to\mathbb{R}$ defined piecewise by polynomials. An *affine spline function* is a special case where each piece is defined by an affine mapping. Such a function can be parameterized by three components: a matrix $\mathbf{A}\in\mathbb{R}^{R\times D}$ representing the slopes of the affine mappings, a vector $\mathbf{b}\in\mathbb{R}^R$ representing the offsets, and a partition $\Omega\triangleq\{\omega_1,\ldots,\omega_R\}$ of the input space \mathbb{R}^D into R regions. For an input $\mathbf{x}\in\mathbb{R}^D$, the affine spline function is defined as:

$$s[\mathbf{A}, \mathbf{b}, \Omega](\mathbf{x}) = \sum_{r=1}^{R} (\langle \mathbf{A}_{r, \cdot}, \mathbf{x} \rangle + \mathbf{b}_r) \mathbf{1}_{\{\mathbf{x} \in \omega_r\}},$$
(1)

where $\mathbf{1}_{\{\mathbf{x}\in\omega_r\}}$ is an indicator function that equals 1 if \mathbf{x} belongs to region ω_r and 0 otherwise.

A max-affine spline function is a special case of an affine spline function that does not need explicit knowledge of Ω . Instead, its output is computed as the maximum value over the affine mappings:

$$s[\mathbf{A}, \mathbf{b}](\mathbf{x}) = \max_{r=1...R} (\langle \mathbf{A}_{r,\cdot}, \mathbf{x} \rangle + \mathbf{b}_r).$$
 (2)

The key result underpinning our study is that many DN layers—such as fully connected and convolutional layers, and convex piecewise-affine activations (e.g., ReLU, max pooling, or maxout)—can be exactly represented as max-affine spline functions [13] (further details in Appendix A).

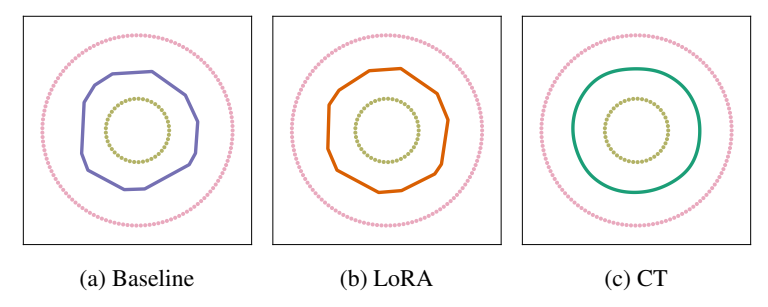


Figure 2: Toy example illustrating how modulating model's activation functions improves local expressivity. The model is a 2-layer MLP with hidden width 7; (a) baseline trained for 4000 steps, then fine-tuned for another 4000 steps using (b) LoRA ($r=1, \alpha=1$) and (c) Trainable CT. CT achieves a near-optimal decision boundary by smoothing the decision boundary of the pretrained model, whereas LoRA only modifies segments of the original piecewise affine boundary.

Now that we have reviewed existing finetuning methods and their limitations, and introduced the necessary spline-based foundations, we proceed to present our proposed method in Section 3.

3 Curvature Tuning (CT): a provable method for model steering

In this section, we introduce our proposed method, Curvature Tuning (CT). We begin by motivating the benefits of modulating decision boundaries as a model steering technique. Then, we dive into CT's construction in Section 3.1 with implementation details in Section 3.2. Additional theoretical intuition is provided in Section 3.3. Extensive experimental validation is presented in Section 4.

Motivating example. Consider a toy binary classification problem in \mathbb{R}^2 , whereby the optimal decision boundary separating two classes is given by the unit circle $S^1 = \{\mathbf{x} \in \mathbb{R}^2 : \|\mathbf{x}\|_2 = 1\}$, parameterized by the curve $\gamma : t \mapsto (\cos 2\pi t, \sin 2\pi t)$, for $t \in [0,1]$. Let $\sigma(z) = \frac{\exp(z)}{1 + \exp(z)}$ be the sigmoid. By definition of decision boundary, an optimal network $f:\mathbb{R}^2\to\mathbb{R}$ should predict both classes with equal probability $\sigma(f(\gamma(t))) = 0.5, \forall t \in [0,1] \iff f(\gamma(t)) = 0.5$ $0, \forall t$. Focusing on the decision boundary, the approximation error e is given by the line integral $e = \int_{\gamma} |f(\mathbf{x})| d\mathbf{x} = \int_{0}^{1} |f(\gamma(t))| \|\gamma'(t)\| dt$. For a ReLU network (Eq. (1)), computing the error over the regions $\Omega_{\gamma} = \Omega \cap S^{1}$ yields $e = \sum_{k=1}^{r'-1} [2\pi t \mathbf{b}_{k} + \mathbf{A}_{k1} \sin 2\pi t - \mathbf{A}_{k2} \cos 2\pi t]_{t_{k}}^{t_{k+1}}$ for $r' = |\Omega_{\gamma}|$, where t_k are the spline breakpoints pulled-back from \mathbb{R}^2 to [0, 1] (full derivations in Appendix C.2). Assuming the network considered attains optimal approximation error, then it is clear that $e \to 0 \iff t_{k+1} \to t_k$, which can only happen when the number of neurons grows to infinity. Importantly, reducing approximation error by adapting the model's weights (either through PEFT or training a larger model from scratch) will still result in an affine spline operator, for which e > 0. This paper explores an orthogonal approach: by modulating the model's activation functions, one can efficiently control the curvature of its decision boundaries, thereby steering them toward optimality—without modifying the model's weights. Fig. 2 illustrates this phenomenon: tuning a model's activation functions can smooth the decision boundary, whereas methods like LoRA can only adjust the segments of the piecewise affine boundary.

3.1 The β -VQ inference framework

This section builds upon the max-affine spline formulation from Eq. (2) to construct a model steering method operating on the model's activation functions. By inspecting Eq. (2), we observe that the mapping remains affine within each (implicitly defined) region where the pointwise maximum does not change. Specifically, for any input \mathbf{x} where $\arg\max_{r=1...R} \left(\langle \mathbf{A}_{r,\cdot}, \mathbf{x} \rangle + \mathbf{b}_r \right)$ remains constant, all such inputs belong to the same region, as they share the same affine mapping. The non-linearity of the function arises when transitioning between these regions.

Smoothing the non-linearity by smoothing the spline region assignment process. Instead of going from one affine mapping to another in an abrupt fashion (whenever crossing that hyperplane), one may consider a smoother transition. There are two common practices to achieve that goal.

We know that each unit of a layer is a max-affine spline. The inference process of each unit can thus be decomposed into two steps:

1. VQ Inference Step (region selection): Determine the affine transformation that maximizes the output, which can be viewed as a vector quantization (VQ) process. The decision is encoded in a one-hot selection variable $\mathbf{t} \in \mathbb{R}^R$, where R is the number of input region partitions of the max-affine spline function, and the r^* -th entry is set to 1, where:

$$r^* = \arg\max_{r \in \{1, \dots, R\}} \left(\langle \mathbf{A}_{r, \cdot}, \mathbf{x} \rangle + \mathbf{b}_r \right). \tag{3}$$

2. Computation Step (affine transformation): Compute the output of the neuron based on the selection variable t:

$$f(\mathbf{x}) = \sum_{r=1}^{R} \mathbf{t}_r \cdot (\langle \mathbf{A}_{r,\cdot}, \mathbf{x} \rangle + \mathbf{b}_r). \tag{4}$$

As discussed, the affine transformation is selected in a *hard* manner, where only the transformation that maximizes the output is chosen. Alternatively, a *soft* selection can be employed, in which the selection variable t is no longer a one-hot vector but is inferred probabilistically. To formalize this, we follow the probabilistic formulation from [28] and introduce the following regularized region selection problem, where the new selection variable \mathbf{t}^{β} is computed as below:

$$\mathbf{t}^{\beta} = \arg \max_{\mathbf{t} \in \Delta_R} \left[\beta \sum_{r=1}^{R} \mathbf{t}_r \cdot (\langle \mathbf{A}_{r,\cdot}, \mathbf{x} \rangle + \mathbf{b}_r) + (1 - \beta) H(\mathbf{t}) \right], \tag{5}$$

where $H(\mathbf{t})$ denotes the Shannon entropy of the selection variable, and Δ_R is the probability simplex in \mathbb{R}^R . The optimal solution \mathbf{t}^{β} has the closed-form:

$$\mathbf{t}_r^{\beta} = \frac{\exp\left(\frac{\beta(\langle \mathbf{A}_{r,\cdot}, \mathbf{x} \rangle + \mathbf{b}_r)}{1 - \beta}\right)}{\sum_{i=1}^{R} \exp\left(\frac{\beta(\langle \mathbf{A}_{i,\cdot}, \mathbf{x} \rangle + \mathbf{b}_i)}{1 - \beta}\right)} \quad \text{for } r = 1, \dots, R.$$
 (6)

Using the computation step in Eq. (4) and a ReLU activation function, switching from $\beta=1$ to $\beta=0.5$ is provably equivalent to replacing ReLU with the Sigmoid Linear Unit (SiLU). In the limit as $\beta\to 0$, the activation function becomes linear—thus making the entire input-output mapping of the network linear as well.

Smoothing the nonlinearity by smoothing the max. As previously mentioned, there is an alternative way to smooth the max-affine spline mapping from Eq. (2). Instead of relying on a soft region assignment, we can instead directly smooth the maximum function. It is already well known that smoothing the maximum operator leads to the log-sum-exp operator (i.e. SoftPlus). Hence, the mapping from Eq. (2) now becomes

$$(1 - \beta) \ln \left[\sum_{r=1}^{R} \exp \left(\frac{\langle \mathbf{A}_{r,\cdot}, \mathbf{x} \rangle + \mathbf{b}_r}{1 - \beta} \right) \right], \tag{7}$$

where we parameterized the mapping so that its behavior is akin to Eq. (5), a value of $\beta \to 1$ recovers the original affine spline activation, e.g., ReLU.

The crucial observation we make is that both parameterizations tend to shift the mean of the output of the unit either by a negative factor (for Eq. (5)) or by a positive factor (for Eq. (7)). This means that in very deep models, varying β with either parameterization produces a shift in the decision boundary or regression that cannot be recovered unless the parameters are trained once again, which we are trying to avoid. As a result, as detailed in Section 3.2, our implementation combines the two parameterizations in a weighted manner to mitigate this bias, as Appendix Fig. 3 illustrates.

3.2 Implementation of CT

We begin by presenting the core activation that gives CT its expressive power—referred to as CT Unit (CTU). The activation is obtained by combining the two parameterizations discussed in Section 3.1,

in order to mitigate the mean shift introduced by each parameterization individually:

$$\varphi_{\beta,c}(\mathbf{x}) = c \cdot \sigma \left(\frac{\beta \mathbf{x}}{1-\beta} \right) \cdot \mathbf{x} + (1-c) \cdot \ln \left[1 + \exp \left(\frac{\mathbf{x}}{1-\beta} \right) \right] \cdot (1-\beta), \tag{8}$$

where $\beta \in [0,1]^2$ modulates the curvature, $c \in [0,1]$ is the mixing coefficient, and $\sigma(\cdot)$ denotes the sigmoid function. This is essentially a convex combination of reparameterized SiLU and SoftPlus:

$$SiLU(\mathbf{x}) = \sigma(\eta \mathbf{x}) \cdot \mathbf{x}, \ \eta = \frac{\beta}{1 - \beta}; \quad SoftPlus(\mathbf{x}) = \frac{1}{\gamma} \cdot \ln\left[1 + \exp\left(\gamma \mathbf{x}\right)\right], \ \gamma = \frac{1}{1 - \beta}. \tag{9}$$

Steering vs Trainable CT. We provide two implementations of CT differing in how CTU is applied. The first, denoted CT, replaces all ReLUs in the network with CTUs using a fixed c=0.5 and a shared $\beta \in [0,1]$. This version is highly parameter-efficient—introducing only a single hyperparameter—and does not require backpropagation, making it suitable as a steering method.

The second, referred to as $Trainable\ CT$, also replaces all ReLUs with CTUs but assigns each output neuron its own trainable pair (β,c) , optimized via backpropagation. This version serves as a finetuning method: while it introduces additional parameters, the increase is modest compared to methods like LoRA and it yields better performance, as shown in Section 4.3. Code for both implementations is provided in Appendix D.

3.3 Curvature Tuning Operates as a Projection

This section provides a characterization of CT, by casting it as a projection of a ReLU network to a space of smooth functions. All proofs are deferred to Appendix C.1.

Theorem 3.1 (Informal). For a ReLU network $f: \mathbb{R}^d \to \mathbb{R}$ with parameter **W** (collecting all weights and biases), for fixed $c \in [0,1]$ and $\beta \in [0,1)$, replacing every instance of ReLU with a CTU (Eq. (8) with hyperparameters β , c is equivalent to projecting f to a smooth function $f_{\beta,c}$ with bounded gradients and curvature, while keeping **W** fixed. Importantly, for $0 < \beta < 1$, $f_{\beta,c}$ enjoys higher local expressivity than f for the same parameter **W**, due to non-vanishing local curvature.

To conclude, we observe how varying β modulates the curvature of the whole model function f and, in turn, of the model's decision boundaries. We begin by noting that for a deep network $f: \mathbb{R}^d \to \mathbb{R}^k$, the decision boundary between any class i and j is given by $\{\mathbf{x} \in \mathbb{R}^d: g(\mathbf{x}) := f_i(\mathbf{x}) - f_j(\mathbf{x}) = 0\}$, for any $i, j = 1, \ldots, k$ with $i \neq j$. Particularly, g is itself a deep network, sharing the same parameters as f up until the penultimate layer, after which the parameter is the vector $W_i^L - W_j^L$ and bias $\mathbf{b}_i^L - \mathbf{b}_j^L$. Importantly, when varying β while keeping all model parameters fixed, the Jacobian $\nabla_{\mathbf{x}} g(\mathbf{x})$ and the Hessian $\nabla_{\mathbf{x}}^2 g(\mathbf{x})$ are respectively given by the gradients and Hessian of $\mathbf{z}^{L-1}(\mathbf{x})$ -corresponding to the post-activation output of the L-1-th layer – weighted by $W_i^L - W_j^L$. Hence, modulating the non-linearity of activation functions via β directly controls the curvature of both model function and its decision boundaries. 3

Particularly, for c=1 (Eq. (8)), as $\beta\to 0$, the activation becomes linear. Since modern DNs (e.g. MLP, CNN, RNN) are composed of activation functions interleaved with affine layers, it follows directly that the entire input-output mapping becomes affine when $\beta\to 0$. In this setting, the curvature of the mapping—defined as the norm of its Hessian—becomes zero. As a result, transitioning from the original DN mapping ($\beta=1$) to the linear setting effectively modulates the network decision boundary curvature, reducing it continuously to zero in the limit. For c<1, the model retains non-vanishing local curvature, while the mapping becomes smooth.

4 Enhancing Model Generalization and Robustness with CT

In this section, we empirically validate the effectiveness of CT across multiple settings. We first show that CT improves generalization (Section 4.1) and enhances robustness (Section 4.2). Section 4.3

In practice, we use $\varphi_{\beta,c}(\mathbf{x}) = c \cdot \sigma \left(\frac{\beta \mathbf{x}}{1-\beta+\varepsilon}\right) \cdot \mathbf{x} + (1-c) \cdot \ln\left[1 + \exp\left(\frac{\mathbf{x}}{1-\beta+\varepsilon}\right)\right] \cdot (1-\beta+\varepsilon)$, where $\varepsilon = 10^{-6}$ ensures numerical stability and allows the formulation to remain well-defined at $\beta = 1$.

³In the following, unless specified, we will thus refer interchangeably to the curvature of a DN mapping and that of its decision boundaries, whenever modulating non-linearities via CT.

shows that *Trainable CT* achieves gains comparable to LoRA with fewer parameters. Finally, we demonstrate CT's effectiveness on transformers despite only partial guarantees (Section 4.4). GPU and seed details are provided in Appendix B.

4.1 Improving generalization on downstream datasets with CT

In this subsection, we evaluate the effectiveness of *CT* in improving model generalization on a variety of downstream datasets. Specifically, we transfer ImageNet-pretrained ResNet-18, ResNet-50, and ResNet-152 models to 12 downstream tasks, including Arabic Characters [29], Arabic Digits [30], Beans [31], CUB-200-2011 [32], DTD [33], FashionMNIST [34], FGVC-Aircraft [35], Flowers102 [36], Food101 [37], and three subsets from MedMNIST-PathMNIST, OCTMNIST, and DermaMNIST [38]. Each dataset is split into training, validation, and test sets, with details in Appendix B.1.

To apply CT, we replace all ReLUs in the backbone with CTUs, freeze the model, and train a linear classifier on the penultimate layer. The optimal β is selected via grid search over $\beta \in [0.7,1]$ (step size 0.01) using validation accuracy, and the corresponding test accuracy is reported. For the baseline, we train a linear classifier on the frozen original model and report the test accuracy of the checkpoint that performs best on the validation set. All linear classifiers use the same training setup detailed in Appendix B.1.

Table 1: Mean accuracy (%) over three runs of ImageNet-pretrained ResNet-18/50 when transferred to 12 downstream datasets. The second row under each method indicates the number of trainable parameters (excluding the linear classifier). *CT* outperforms linear probing on the frozen backbone, and *Trainable CT* surpasses LoRA (rank 1). Results for ResNet-152 can be found in Appendix Table 4.

| | | Re | sNet-18 | | ResNet-50 | | | |
|-------------------|--------|-------|---------|----------|-----------|-------|-----------------|----------|
| Dataset | Frozen | CT | LoRA | Train CT | Frozen | CT | LoRA (70442) | Train CT |
| | (0) | (1) | (35923) | (3968) | (0) | (1) | (79443) | (45440) |
| Arabic Characters | 81.91 | 87.65 | 93.37 | 93.76 | 80.65 | 83.66 | 94.21 | 95.67 |
| Arabic Digits | 97.93 | 98.77 | 99.08 | 99.03 | 98.33 | 98.37 | 99.08 | 99.16 |
| Beans | 87.76 | 90.36 | 93.23 | 94.01 | 89.58 | 91.93 | 94.79 | 95.57 |
| CUB-200 | 62.84 | 63.18 | 54.83 | 64.30 | 65.23 | 64.62 | 66.17 | 71.03 |
| DTD | 62.80 | 62.66 | 54.36 | 63.62 | 67.34 | 66.91 | 64.70 | 65.07 |
| FashionMNIST | 88.63 | 88.70 | 91.65 | 91.07 | 90.05 | 90.34 | 92.19 | 92.78 |
| FGVC-Aircraft | 36.80 | 38.68 | 29.19 | 46.44 | 38.03 | 41.16 | 41.99 | 55.70 |
| Flowers102 | 80.86 | 81.97 | 67.53 | 86.55 | 84.00 | 83.84 | 82.58 | 87.62 |
| Food101 | 61.41 | 62.27 | 64.40 | 66.04 | 68.06 | 68.02 | 71.42 | 73.60 |
| DermaMNIST | 74.83 | 75.05 | 74.21 | 77.66 | 75.94 | 75.89 | 75.73 | 78.02 |
| OCTMNIST | 65.03 | 67.27 | 74.27 | 69.53 | 67.53 | 68.00 | 75.90 | 74.13 |
| PathMNIST | 86.77 | 87.51 | 87.62 | 87.17 | 90.08 | 90.26 | 85.43 | 87.33 |
| Average | 73.96 | 75.34 | 73.64 | 78.26 | 76.24 | 76.92 | 78.68 | 81.31 |

Table 1 and Appendix Table 4 show mean accuracy over three runs for linear probing with and without *CT* on 12 downstream datasets using ResNet-18/50/152 backbones. *CT* consistently improves generalization, with average relative gains of 1.97%, 1.16%, and 0.02% respectively.

We also report the average optimal β across datasets: 0.84 for ResNet-18, 0.94 for ResNet-50, and 0.96 for ResNet-152 (full results in Appendix Table 5). These values are consistently close to 1, suggesting the search range can be narrowed for efficiency. The upward trend with model size indicates that larger models require less curvature adjustment, which is intuitive as deeper networks can approximate complex curvature more effectively. Example accuracy curves in Appendix Fig. 4 show that accuracy varies smoothly with β and typically peaks in the middle of the search range.

4.2 Improving robustness on adversarial and corrupted data with CT

In this subsection, we demonstrate that CT can enhance model robustness using benchmarks from RobustBench [14]. We evaluate robustness of ResNet-18, ResNet-50 and ResNet-152 on CIFAR-10, CIFAR-100, and ImageNet using the official ℓ_2 and ℓ_∞ adversarial benchmarks from RobustBench

[14], as well as the common corruption benchmark [39], which contains naturally perturbed images. For specific evaluation configurations, see Appendix B.2.

It is worth noting that here we apply CT in a straightforward manner to assess its robustness benefits, without focusing on how to find the optimal β value. Specifically, we replace all ReLU activations in the backbone with CTUs and perform a grid search over $\beta \in [0.7,1]$ with a step size of 0.01. We report the value that achieves the best performance on each benchmark.

Table 2: Mean robust accuracy (%) over three runs of ImageNet-pretrained ResNet-18/50/152 under ℓ_2/ℓ_∞ attacks and corruptions on CIFAR-10/100 and ImageNet. *CT* yields substantial improvements under ℓ_∞ attacks, moderate gains under ℓ_2 attacks, and marginal improvements under common corruptions, with the selected β values generally close to 1.

| | | ℓ_2 | | ℓ_∞ | | | Corruption | | | |
|-----------|----------|----------|-------|---------------|-------|-------|------------|-------|-------|------|
| Model | Dataset | Base | CT | β | Base | CT | β | Base | CT | β |
| | CIFAR10 | 53.67 | 53.67 | 1.00 | 11.17 | 14.93 | 0.90 | 77.73 | 77.73 | 1.00 |
| ResNet18 | CIFAR100 | 24.30 | 25.50 | 0.92 | 4.47 | 6.90 | 0.92 | 51.81 | 51.95 | 0.94 |
| | ImageNet | 23.37 | 23.37 | 1.00 | 0.00 | 7.00 | 0.89 | 33.11 | 33.32 | 0.92 |
| | Average | 33.78 | 34.18 | 0.97 | 5.21 | 9.61 | 0.90 | 54.22 | 54.33 | 0.95 |
| | CIFAR10 | 55.10 | 56.53 | 0.97 | 10.10 | 12.08 | 0.90 | 77.26 | 77.26 | 1.00 |
| ResNet50 | CIFAR100 | 23.83 | 25.80 | 0.96 | 4.43 | 7.90 | 0.93 | 53.91 | 53.93 | 0.98 |
| | ImageNet | 31.90 | 31.90 | 1.00 | 0.30 | 9.30 | 0.93 | 39.64 | 39.64 | 1.00 |
| | Average | 36.94 | 38.08 | 0.98 | 4.94 | 10.68 | 0.94 | 56.94 | 56.94 | 0.99 |
| | CIFAR10 | 56.27 | 56.27 | 1.00 | 11.47 | 15.00 | 0.99 | 78.82 | 78.83 | 0.99 |
| ResNet152 | CIFAR100 | 27.90 | 28.23 | 0.98 | 5.40 | 7.70 | 0.99 | 56.12 | 56.12 | 1.00 |
| | ImageNet | 42.50 | 42.50 | 1.00 | 0.30 | 13.53 | 0.97 | 45.47 | 45.47 | 0.99 |
| | Average | 42.22 | 42.33 | 0.99 | 5.72 | 12.08 | 0.98 | 60.14 | 60.14 | 0.99 |

As summarized in Table 2, CT is particularly effective against ℓ_{∞} attacks, achieving large relative improvements of 44.01%, 1032.64%, and 1494.46% for ResNet-18, ResNet-50, and ResNet-152, respectively.⁴ The improvements under ℓ_2 attacks are moderate—1.65%, 3.62%, and 0.39%—while the gains on corruption robustness are marginal. The corresponding average optimal β values, also shown in Table 2, are consistently close to 1. This suggests that modest curvature modulation is sufficient to achieve improved robustness, showing again the efficiency of CT in practice.

4.3 Trainable CT is comparable to LoRA

In this subsection, we show that $Trainable\ CT$ further improves generalization, achieving performance comparable to LoRA with fewer parameters. We conduct experiments using the same setup as in Section 4.1, evaluating both $Trainable\ CT$ and LoRA. For both methods, we replace the original linear classifier in each model with an appropriate one, and apply the respective method to the pretrained backbone. In $Trainable\ CT$, we initialize all β parameters to 0.8 and all c parameters to 0.5. For LoRA, we set the rank r=1 and scale $\alpha=1$, focusing on the comparison rather than tuning LoRA's hyperparameters. We apply LoRA to all convolutional and linear layers in the backbone, and provide implementation details in Appendix E. Refer to Appendix B.3 for training configurations we apply for the two methods. Here we report the test accuracy of the best checkpoint on the validation set.

The results, summarized in Table 1 and Appendix Table 4, show that $Trainable\ CT$ achieves the highest performance across all methods, with average relative improvements on ResNet-18, 50, and 152 of 6.75%, 8.59%, and 8.34% over the baseline; 4.62%, 7.14%, and 8.51% over CT; and 10.20%, 4.64%, and 1.70% over LoRA. Importantly, $Trainable\ CT$ achieves better performance than LoRA with fewer parameters. As reported in Table 1 and Appendix Table 4, the number of trainable parameters (excluding the classifier) used by $Trainable\ CT$ amounts to only 11.05%, 57.20%, and 59.09% of that used by LoRA on ResNet-18, 50, and 152, respectively—even with LoRA operating at its lowest-rank setting (r=1). This highlights the parameter efficiency of our approach.

 $^{^4}$ We exclude the ResNet-18 result on ImageNet under ℓ_{∞} from this computation since the baseline robust accuracy is 0.

To better understand how *Trainable CT* behaves during training, we analyze the distributions of learned β and c values (full statistics provided in Appendix Tables 6 and 7). We observe a high degree of within-model variation, with standard deviations ranging from 0.31 to 0.38, while the means remain remarkably stable across architectures: 0.69 to 0.74 for β and 0.57 to 0.59 for c. These mean values are close to those used in CT, though the learned β values tend to be smaller than the optimal shared β found in CT (0.84 to 0.96), while the learned c values are larger than the fixed c = 0.5.

We further visualize the distributions in Appendix Figs. 5 and 6. In most datasets, as shown in Appendix Fig. 5 (OCTMNIST), both β and c exhibit a sharp U-shaped distribution—concentrating near 0 and 1 with a flat middle. This suggests that *Trainable CT* leverages its parameter flexibility to assign values at the extremes, producing an effective average close to the manually chosen settings in CT, rather than concentrating around the mean values themselves. In a few datasets, we observe deviations from this trend, as exemplified in Appendix Fig. 6 (DTD). Nonetheless, a consistent pattern is that for any given dataset, the distributions remain visually similar across all models.

4.4 CT shows promise on transformers and emerging architectures

In this subsection, we investigate the effectiveness of CT on transformer architectures. Unlike ResNets, transformers include attention layers that fall outside the max-affine spline framework, weakening theoretical guarantees. However, the feed-forward blocks with convex, piecewise-affine activations (e.g., ReLU) still retain them.

While our method is naturally suited for ReLU activations, most transformers use activation functions such as GELU. To bridge this gap, we replace all GELUs in Swin-T and Swin-S with ReLU, and pretrain the models from scratch on Imagenette (details can be found in Appendix B.4). Then as before, we transfer the models to the same 12 downstream datasets and apply all four methods: the frozen baseline, CT, LoRA, and $Trainable\ CT$. The transfer protocols remain identical to those in Section 4.1 and Section 4.3, except that LoRA is now applied to all QKV projection layers.

Table 3: Mean accuracy (%) over three runs of Imagenette-pretrained Swin-T/S when transferred to 12 downstream datasets. The second row under each method indicates the number of trainable parameters (excluding the linear classifier). *CT* outperforms linear probing on Swin-T, while *Trainable CT* significantly improves over linear probing on both models but underperforms LoRA.

| | Swin-T | | | | Swin-S | | | |
|-------------------|--------|-------|---------|----------|--------|-------|----------|----------|
| Dataset | Frozen | CT | LoRA | Train CT | Frozen | CT | LoRA | Train CT |
| | (0) | (1) | (74832) | (532) | (0) | (1) | (148560) | (868) |
| Arabic Characters | 30.67 | 31.08 | 56.32 | 41.95 | 31.81 | 31.16 | 62.16 | 40.88 |
| Arabic Digits | 83.71 | 85.24 | 97.54 | 90.82 | 80.74 | 81.11 | 97.91 | 91.44 |
| Beans | 60.68 | 61.46 | 75.52 | 68.49 | 55.99 | 54.43 | 73.96 | 67.71 |
| CUB-200 | 4.82 | 4.87 | 7.42 | 6.09 | 4.46 | 4.02 | 9.19 | 6.71 |
| DTD | 15.92 | 15.90 | 16.99 | 17.04 | 16.03 | 15.78 | 18.67 | 17.66 |
| FashionMNIST | 73.81 | 74.01 | 83.90 | 77.07 | 73.28 | 73.29 | 86.15 | 75.76 |
| FGVC-Aircraft | 4.57 | 4.47 | 5.59 | 6.14 | 4.61 | 4.74 | 6.55 | 6.16 |
| Flowers102 | 14.09 | 14.01 | 16.66 | 16.53 | 12.93 | 13.12 | 17.28 | 17.99 |
| Food101 | 14.85 | 14.79 | 18.17 | 15.20 | 14.22 | 14.28 | 19.41 | 14.50 |
| DermaMNIST | 70.24 | 70.99 | 74.08 | 71.37 | 69.23 | 70.34 | 73.93 | 70.59 |
| OCTMNIST | 49.60 | 51.37 | 63.53 | 53.23 | 48.07 | 47.93 | 63.90 | 51.23 |
| PathMNIST | 76.73 | 77.78 | 81.31 | 77.35 | 74.82 | 76.54 | 76.62 | 78.59 |
| Average | 41.64 | 42.16 | 49.75 | 45.11 | 40.52 | 40.56 | 50.48 | 44.94 |

The results, shown in Table 3, indicate that *CT* yields a modest average relative improvement of 0.68% over the frozen baseline on Swin-T, but slightly underperforms the baseline by 0.58% on Swin-S. In contrast, *Trainable CT* delivers substantial improvements, outperforming the baseline by 13.32% and 17.93% on Swin-T and Swin-S. Despite these gains, *Trainable CT* underperforms LoRA in this setting, trailing by 8.29% and 11.89% on Swin-T and Swin-S. We attribute this performance gap to two main factors. First, as shown in Table 3, *Trainable CT* introduces only 0.71% and 0.58%

⁵This behavior may in part be influenced by the sigmoid-based parameterization used in our implementation of *Trainable CT* to constrain β and c during training.

as many trainable parameters as LoRA on Swin-T and Swin-S—a much lower ratio than in the ResNet experiments. Second, the pretraining dataset, Imagenette, is relatively small, containing only 10 classes and 9,469 training samples. This limited scale may lead to underpowered representations for downstream transfer, as reflected in the overall low baseline accuracy across datasets. In such settings, LoRA's higher capacity may allow it to more effectively adapt the pretrained model to diverse downstream tasks. Thus though *Trainable CT* is outperformed by LoRA in this scenario, the results still demonstrate the potential of CT in transformer models.

Moreover, recent work advocating a return to ReLU in transformers [40] suggests that CT can be applied to a broader class of state-of-the-art architectures with minimal modification. Finally, although our experiments focus on ReLU-based networks, CT is readily extensible to architectures using SiLU or Softplus activations, as both are special cases of the general CTU formulation in Eq. (8). This includes emerging models like Mamba [41], which uses SiLU.

5 Conclusion

In this paper, we propose Curvature Tuning (CT), an interpretable and principled model steering method that provably modulates a model's decision boundary via a single parameter injected into its activation functions without changing the model weights. Theoretically, we show that CT modulates the model's nonlinearities and more essentially projects the model onto a space of smooth functions, offering a complementary view to existing PEFT methods. Practically, we apply CT in two forms: as a steering method with fixed parameters (CT) and as a finetuning method with learnable ones (Trainable CT). Both improve generalization, with Trainable CT approaching LoRA's performance. We also show that CT enhances robustness.

Our work has limitations that open avenues for future research. For instance, while our focus is on ReLU-based networks, CT is compatible with activations like Softplus or SiLU (e.g., in Mamba), which warrants further study. Additionally, analyzing the layer-wise distribution of β and c in *Trainable CT* may shed light on how different layers contribute to representation and abstraction.

Broader impacts

This paper presents work whose goal is to advance the field of deep learning. There are many potential societal consequences of our work, none of which we feel must be specifically highlighted here.

References

- [1] Abhimanyu Dubey, Abhinav Jauhri, Abhinav Pandey, Abhishek Kadian, Ahmad Al-Dahle, Aiesha Letman, Akhil Mathur, Alan Schelten, Amy Yang, Angela Fan, et al. The llama 3 herd of models. *arXiv preprint arXiv:2407.21783*, 2024.
- [2] Maxime Oquab, Timothée Darcet, Théo Moutakanni, Huy Vo, Marc Szafraniec, Vasil Khalidov, Pierre Fernandez, Daniel Haziza, Francisco Massa, Alaaeldin El-Nouby, et al. Dinov2: Learning robust visual features without supervision. *arXiv preprint arXiv:2304.07193*, 2023.
- [3] Alec Radford, Jong Wook Kim, Chris Hallacy, Aditya Ramesh, Gabriel Goh, Sandhini Agarwal, Girish Sastry, Amanda Askell, Pamela Mishkin, Jack Clark, Gretchen Krueger, and Ilya Sutskever. Learning transferable visual models from natural language supervision, 2021. URL https://arxiv.org/abs/2103.00020.
- [4] Xiaohua Zhai, Basil Mustafa, Alexander Kolesnikov, and Lucas Beyer. Sigmoid loss for language image pre-training. In *Proceedings of the IEEE/CVF International Conference on Computer Vision*, pages 11975–11986, 2023.
- [5] Moo Jin Kim, Karl Pertsch, Siddharth Karamcheti, Ted Xiao, Ashwin Balakrishna, Suraj Nair, Rafael Rafailov, Ethan Foster, Grace Lam, Pannag Sanketi, et al. Openvla: An open-source vision-language-action model. *arXiv preprint arXiv:2406.09246*, 2024.
- [6] Alec Radford. Improving language understanding by generative pre-training. 2018.

- [7] Ahmadreza Jeddi, Mohammad Javad Shafiee, and Alexander Wong. A simple fine-tuning is all you need: Towards robust deep learning via adversarial fine-tuning. *arXiv preprint arXiv:2012.13628*, 2020.
- [8] Neil Houlsby, Andrei Giurgiu, Stanislaw Jastrzebski, Bruna Morrone, Quentin de Laroussilhe, Andrea Gesmundo, Mona Attariyan, and Sylvain Gelly. Parameter-efficient transfer learning for nlp, 2019. URL https://arxiv.org/abs/1902.00751.
- [9] Edward J. Hu, Yelong Shen, Phillip Wallis, Zeyuan Allen-Zhu, Yuanzhi Li, Shean Wang, Lu Wang, and Weizhu Chen. Lora: Low-rank adaptation of large language models, 2021. URL https://arxiv.org/abs/2106.09685.
- [10] Kurt Hornik, Maxwell Stinchcombe, and Halbert White. Multilayer feedforward networks are universal approximators. *Neural networks*, 2(5):359–366, 1989.
- [11] George Cybenko. Approximation by superpositions of a sigmoidal function. *Mathematics of control, signals and systems*, 2(4):303–314, 1989.
- [12] Guido F Montufar, Razvan Pascanu, Kyunghyun Cho, and Yoshua Bengio. On the number of linear regions of deep neural networks. Advances in neural information processing systems, 27, 2014.
- [13] Randall Balestriero and Richard Baraniuk. A spline theory of deep learning. In Jennifer Dy and Andreas Krause, editors, *Proceedings of the 35th International Conference on Machine Learning*, volume 80 of *Proceedings of Machine Learning Research*, pages 374–383. PMLR, 10–15 Jul 2018. URL https://proceedings.mlr.press/v80/balestriero18b.html.
- [14] Francesco Croce, Maksym Andriushchenko, Vikash Sehwag, Edoardo Debenedetti, Nicolas Flammarion, Mung Chiang, Prateek Mittal, and Matthias Hein. Robustbench: a standardized adversarial robustness benchmark. *arXiv preprint arXiv:2010.09670*, 2020.
- [15] Mathilde Caron, Hugo Touvron, Ishan Misra, Hervé Jégou, Julien Mairal, Piotr Bojanowski, and Armand Joulin. Emerging properties in self-supervised vision transformers. In *Proceedings of the IEEE/CVF international conference on computer vision*, pages 9650–9660, 2021.
- [16] Zeyu Han, Chao Gao, Jinyang Liu, Jeff Zhang, and Sai Qian Zhang. Parameter-efficient fine-tuning for large models: A comprehensive survey. *arXiv preprint arXiv:2403.14608*, 2024.
- [17] Xiang Lisa Li and Percy Liang. Prefix-tuning: Optimizing continuous prompts for generation. *arXiv preprint arXiv:2101.00190*, 2021.
- [18] Haokun Liu, Derek Tam, Mohammed Muqeeth, Jay Mohta, Tenghao Huang, Mohit Bansal, and Colin A Raffel. Few-shot parameter-efficient fine-tuning is better and cheaper than in-context learning. *Advances in Neural Information Processing Systems*, 35:1950–1965, 2022.
- [19] Baohao Liao and Christof Monz. 3-in-1: 2d rotary adaptation for efficient finetuning, efficient batching and composability. *arXiv* preprint arXiv:2409.00119, 2024.
- [20] Demi Guo, Alexander M Rush, and Yoon Kim. Parameter-efficient transfer learning with diff pruning. *arXiv preprint arXiv:2012.07463*, 2020.
- [21] Mojtaba Valipour, Mehdi Rezagholizadeh, Ivan Kobyzev, and Ali Ghodsi. Dylora: Parameter efficient tuning of pre-trained models using dynamic search-free low-rank adaptation. *arXiv* preprint arXiv:2210.07558, 2022.
- [22] Yuning Mao, Lambert Mathias, Rui Hou, Amjad Almahairi, Hao Ma, Jiawei Han, Wen-tau Yih, and Madian Khabsa. Unipelt: A unified framework for parameter-efficient language model tuning. *arXiv preprint arXiv:2110.07577*, 2021.
- [23] Jiaao Chen, Aston Zhang, Xingjian Shi, Mu Li, Alex Smola, and Diyi Yang. Parameter-efficient fine-tuning design spaces. *arXiv preprint arXiv:2301.01821*, 2023.
- [24] Chongyang Gao, Kezhen Chen, Jinmeng Rao, Baochen Sun, Ruibo Liu, Daiyi Peng, Yawen Zhang, Xiaoyuan Guo, Jie Yang, and VS Subrahmanian. Higher layers need more lora experts. *arXiv preprint arXiv:2402.08562*, 2024.

- [25] Shuaijun Chen, Omid Tavallaie, Niousha Nazemi, Xin Chen, and Albert Y Zomaya. Autorank: Mcda based rank personalization for lora-enabled distributed learning. arXiv preprint arXiv:2412.15553, 2024.
- [26] Damjan Kalajdzievski. A rank stabilization scaling factor for fine-tuning with lora. arXiv preprint arXiv:2312.03732, 2023.
- [27] Soufiane Hayou, Nikhil Ghosh, and Bin Yu. The impact of initialization on lora finetuning dynamics. *arXiv* preprint arXiv:2406.08447, 2024.
- [28] Randall Balestriero and Richard G. Baraniuk. From hard to soft: Understanding deep network nonlinearities via vector quantization and statistical inference, 2018. URL https://arxiv. org/abs/1810.09274.
- [29] Ahmed El-Sawy, Mohamed Loey, and Hazem El-Bakry. Arabic handwritten characters recognition using convolutional neural network. WSEAS Transactions on Computer Research, 5:11–19, 2017.
- [30] Ahmed El-Sawy, EL-Bakry Hazem, and Mohamed Loey. Cnn for handwritten arabic digits recognition based on lenet-5. In *International conference on advanced intelligent systems and informatics*, pages 566–575. Springer, 2016.
- [31] Makerere AI Lab. Bean Disease Dataset, January 2020. URL https://github.com/ AI-Lab-Makerere/ibean/.
- [32] C. Wah, S. Branson, P. Welinder, P. Perona, and S. Belongie. The caltech-ucsd birds-200-2011 dataset. Technical Report CNS-TR-2011-001, California Institute of Technology, 2011.
- [33] M. Cimpoi, S. Maji, I. Kokkinos, S. Mohamed, , and A. Vedaldi. Describing textures in the wild. In *Proceedings of the IEEE Conf. on Computer Vision and Pattern Recognition (CVPR)*, 2014.
- [34] Han Xiao, Kashif Rasul, and Roland Vollgraf. Fashion-mnist: a novel image dataset for benchmarking machine learning algorithms. *arXiv preprint arXiv:1708.07747*, 2017.
- [35] Subhransu Maji, Esa Rahtu, Juho Kannala, Matthew Blaschko, and Andrea Vedaldi. Fine-grained visual classification of aircraft. *arXiv preprint arXiv:1306.5151*, 2013.
- [36] Maria-Elena Nilsback and Andrew Zisserman. Automated flower classification over a large number of classes. In 2008 Sixth Indian conference on computer vision, graphics & image processing, pages 722–729. IEEE, 2008.
- [37] Lukas Bossard, Matthieu Guillaumin, and Luc Van Gool. Food-101 mining discriminative components with random forests. In *European Conference on Computer Vision*, 2014.
- [38] Jiancheng Yang, Rui Shi, Donglai Wei, Zequan Liu, Lin Zhao, Bilian Ke, Hanspeter Pfister, and Bingbing Ni. Medmnist v2-a large-scale lightweight benchmark for 2d and 3d biomedical image classification. *Scientific Data*, 10(1):41, 2023.
- [39] Dan Hendrycks and Thomas Dietterich. Benchmarking neural network robustness to common corruptions and perturbations. *arXiv preprint arXiv:1903.12261*, 2019.
- [40] Iman Mirzadeh, Keivan Alizadeh, Sachin Mehta, Carlo C Del Mundo, Oncel Tuzel, Golnoosh Samei, Mohammad Rastegari, and Mehrdad Farajtabar. Relu strikes back: Exploiting activation sparsity in large language models. *arXiv preprint arXiv:2310.04564*, 2023.
- [41] Albert Gu and Tri Dao. Mamba: Linear-time sequence modeling with selective state spaces. *arXiv preprint arXiv:2312.00752*, 2023.

Appendix

The remainder of the paper collects additional experimental validation and theoretical derivations supporting our main results. The appendix is organized as follows.

- 1. Appendix A briefly connects several deep network architectures to affine spline operators.
- 2. Appendix B details our experimental setup.
- 3. Appendix C provides theoretical intuition behind CT.
- 4. Appendix D provides pseudocode for CT as well as Trainable CT.
- 5. Appendix E provides pseudocode for LoRA, describing how the method was applied throughout our experiments (Section 4).

A Spline Theory

The spline theory of deep learning establishes that a large class of deep network (DN) layers can be modeled as Max Affine Spline Operators (MASOs). More precisely:

Theorem A.1. (Propositions 1-4 in Balestriero and Baraniuk [13]) Any DN layer comprising a linear operator (e.g., fully connected or convolutional layer) followed by a convex and piecewise affine non-linear operator (e.g., ReLU, leaky-ReLU, absolute value activation, max/average/channel pooling, maxout; with or without skip connections) is a MASO.

Consequently, a deep network (e.g., MLP, CNN, RNN, ResNet) composed of such linear operators and convex, piecewise affine non-linear operators is a composition of MASOs. However, it is important to note that the network as a whole is not a MASO but an Affine Spline Operator (ASO). In other words, conditioned on the input, such deep networks are equivalent to an affine transformation, but globally, the transformation is not convex.

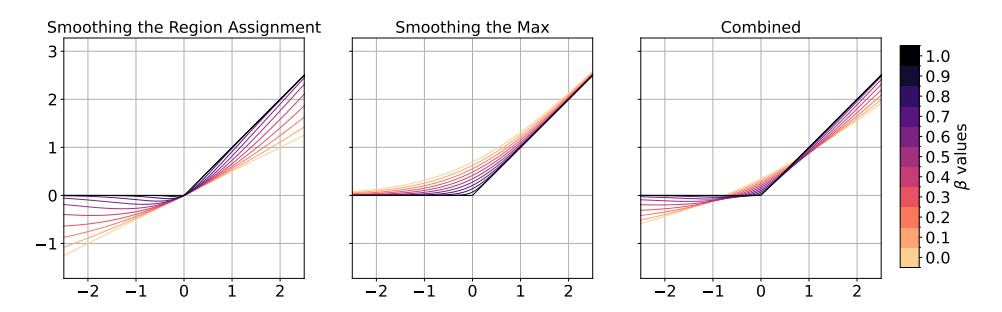


Figure 3: Visualization of non-linearity smoothing through region assignment smoothing, max smoothing, and their combination. The combined approach mitigates the opposing biases introduced by the individual methods.

Building on the MASO interpretation, curvature tuning proposes to smoothen non-linearities (e.g. ReLU) of a DN as a novel form of model steering, that avoids retraining or fine-tuning the learned layers. By recalling Section 3.1, when smoothing is performed by applying Eq. (5) or Eq. (7) to a DN layer (interpreted as a MASO), the layer's output is statistically biased by either a negative or a positive factor, respectively. In order to counter the bias without retraining, a convex combination of the two equations is used, as shown in Fig. 3 for different values of β .

B Supplementary experimental details

This section provides additional experimental setup details and results, organized to correspond with the subsections in Section 4.

All experiments were conducted using 8 RTX 3090 GPUs and one L40 GPU, with runs performed under random seeds 42, 43, and 44.

B.1 Improving generalization on downstream datasets with CT (Section 4.1)

For each of the 12 downstream datasets, we split the data into training, validation, and test sets. If a dataset does not include a validation set, we hold out 20% of the training data using stratified sampling. Otherwise, we use the original validation split provided.

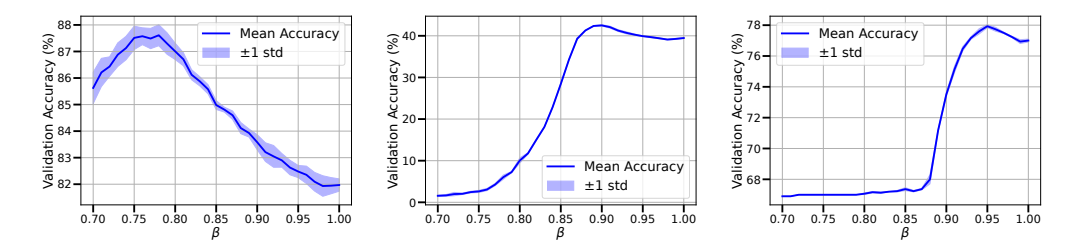
All linear classifiers are trained for 20 epochs using the Adam optimizer with a learning rate of 10^{-3} . We apply linear warm-up during the first epoch and decay the learning rate by a factor of 10 after epoch 10.

Additional results are provided as follows:

- Table 4: mean accuracy over three runs of ImageNet-pretrained ResNet-152 when transferred to 12 downstream datasets, comparing linear probing with and without *CT*.
- Table 5: average optimal β values for CT across three runs.
- Fig. 4: example validation accuracy vs. β curves over three runs for CT.

Table 4: Mean accuracy (%) over three runs of ImageNet-pretrained ResNet-152 when transferred to 12 downstream datasets. The second row under each method indicates the number of trainable parameters (excluding the linear classifier). *CT* outperforms linear probing on the frozen backbone, and *Trainable CT* surpasses LoRA (rank 1).

| Dataset | Frozen (0) | <i>CT</i> (1) | LoRA (243283) | <i>Train CT</i> (143744) |
|-------------------|------------|---------------|---------------|--------------------------|
| | (0) | (1) | (243263) | (143/44) |
| Arabic Characters | 79.86 | 79.21 | 95.96 | 96.47 |
| Arab Digits | 98.07 | 98.15 | 99.15 | 99.10 |
| Beans | 87.50 | 87.50 | 93.75 | 96.35 |
| CUB-200 | 67.68 | 68.15 | 70.59 | 73.04 |
| DTD | 66.97 | 66.99 | 66.63 | 63.39 |
| FashionMNIST | 90.44 | 90.51 | 92.77 | 93.39 |
| FGVC-aircraft | 38.74 | 38.51 | 48.84 | 58.16 |
| Flowers 102 | 82.98 | 83.28 | 84.40 | 83.43 |
| Food101 | 71.11 | 71.13 | 74.66 | 76.08 |
| DermaMNIST | 75.68 | 76.23 | 76.91 | 77.94 |
| OCTMNIST | 69.27 | 69.10 | 76.43 | 75.17 |
| PathMNIST | 89.91 | 89.82 | 84.94 | 83.60 |
| Average | 76.52 | 76.55 | 80.42 | 81.34 |



(a) ResNet-18 on Arabic Characters (b) ResNet-50 on FGVC-Aircraft (c) ResNet-152 on DermaMNIST

Figure 4: Validation accuracy (%) of CT during the β search, averaged over three runs. The accuracy curve varies smoothly and typically peaks in the middle of the β range.

B.2 Improving robustness on adversarial and corrupted data with CT (Section 4.2)

Due to computational constraints, we evaluate each benchmark using 1,000 samples. For adversarial evaluations, we follow the official RobustBench settings: $\varepsilon_2=0.5$ for ℓ_2 attacks and $\varepsilon_\infty=\frac{8}{255}$ for ℓ_∞ attacks.

Table 5: Mean β of CT over three runs of ImageNet-pretrained ResNet-18/50/152 and Imagenette-pretrained Swin-T/S when transferred to 12 downstream datasets. The learned β values are consistently high (ranging from 0.84 to 0.96 across models), and tend to be larger for larger models.

| Dataset | ResNet-18 | ResNet-50 | ResNet-152 | Swin-T | Swin-S |
|-------------------|-----------|-----------|------------|--------|--------|
| Arabic Characters | 0.77 | 0.89 | 0.96 | 0.92 | 0.97 |
| Arabic Digits | 0.75 | 0.93 | 0.95 | 0.86 | 0.96 |
| Beans | 0.76 | 0.94 | 0.97 | 0.94 | 0.98 |
| CUB-200 | 0.91 | 0.93 | 0.94 | 0.97 | 0.87 |
| DTD | 0.88 | 0.98 | 0.98 | 0.96 | 0.95 |
| FashionMNIST | 0.92 | 0.95 | 0.96 | 0.89 | 0.98 |
| FGVC-Aircraft | 0.82 | 0.90 | 0.95 | 0.93 | 0.97 |
| Flowers 102 | 0.84 | 0.96 | 0.95 | 0.99 | 0.97 |
| Food101 | 0.87 | 0.98 | 0.99 | 0.97 | 0.99 |
| DermaMNIST | 0.94 | 0.95 | 0.95 | 0.93 | 0.89 |
| OCTMNIST | 0.80 | 0.94 | 0.98 | 0.88 | 0.95 |
| PathMNIST | 0.83 | 0.96 | 0.92 | 0.90 | 0.94 |
| Average | 0.84 | 0.94 | 0.96 | 0.93 | 0.95 |

B.3 *Trainable CT* is comparable to LoRA (Section 4.3)

Both *Trainable CT* and LoRA are trained for 20 epochs using the Adam optimizer. To ensure proper convergence, we use different learning rates: for *Trainable CT*, a learning rate of 10^{-1} is applied to the (β, c) parameters and 10^{-3} to the linear classifier; for LoRA, a learning rate of 10^{-4} is used for both the adapter parameters and the classifier. As before, we apply linear warm-up during the first epoch and decay the learning rate by a factor of 10 after epoch 10.

Additional results are provided as follows:

- Table 4: mean accuracy over three runs of ImageNet-pretrained ResNet-152 when transferred to 12 downstream datasets, comparing LoRA and *Trainable CT*.
- Tables 6 and 7: mean and standard deviation of the learned β and c values for $Trainable\ CT$ across three runs.
- Figs. 5 and 6: example distributions of β and c values in *Trainable CT*, illustrating commonly and uncommonly observed patterns.

B.4 CT shows promise on transformers and emerging architectures (Section 4.4)

For the pretraining of Swin-T and Swin-S, we train both models for 200 epochs with a batch size of 128. Training is performed using SGD with a learning rate of 0.1, momentum of 0.9, and weight decay of 5×10^{-4} . We apply linear warm-up during the first epoch and decay the learning rate by a factor of 0.2 at epochs 60, 120, and 160. Training and validation accuracy curves are shown in Fig. 7.

Table 6: Distribution of β values in *Trainable CT*, computed over all β parameters across all three runs of ImageNet-pretrained ResNet-18/50/152 and Imagenette-pretrained Swin-T/S when transferred to 12 downstream datasets. The mean and standard deviation of β are similar across models (means between 0.69–0.77, stds between 0.31–0.37), suggesting consistent tuning behavior at the model level, while the relatively large standard deviations indicate substantial variation of β within each network.

| Dataset | ResNet-18 | ResNet-50 | ResNet-152 | Swin-T | Swin-S |
|-------------------|-----------------|-----------------|-----------------|-----------------|-----------------|
| Arabic Characters | 0.72 ± 0.34 | 0.65 ± 0.41 | 0.68 ± 0.39 | 0.73 ± 0.35 | 0.76 ± 0.33 |
| Arabic Digits | 0.70 ± 0.43 | 0.62 ± 0.48 | 0.62 ± 0.47 | 0.65 ± 0.42 | 0.64 ± 0.43 |
| Beans | 0.72 ± 0.26 | 0.76 ± 0.23 | 0.77 ± 0.19 | 0.79 ± 0.24 | 0.83 ± 0.23 |
| CUB-200 | 0.81 ± 0.17 | 0.76 ± 0.29 | 0.79 ± 0.29 | 0.82 ± 0.27 | 0.83 ± 0.28 |
| DTD | 0.78 ± 0.19 | 0.77 ± 0.25 | 0.79 ± 0.24 | 0.87 ± 0.17 | 0.88 ± 0.19 |
| FashionMNIST | 0.72 ± 0.41 | 0.65 ± 0.46 | 0.63 ± 0.46 | 0.67 ± 0.42 | 0.66 ± 0.43 |
| FGVC-Aircraft | 0.75 ± 0.23 | 0.70 ± 0.33 | 0.74 ± 0.32 | 0.81 ± 0.25 | 0.82 ± 0.27 |
| Flowers102 | 0.75 ± 0.16 | 0.75 ± 0.21 | 0.79 ± 0.17 | 0.81 ± 0.22 | 0.84 ± 0.22 |
| Food101 | 0.80 ± 0.30 | 0.71 ± 0.43 | 0.76 ± 0.40 | 0.78 ± 0.36 | 0.74 ± 0.40 |
| DermaMNIST | 0.74 ± 0.34 | 0.70 ± 0.39 | 0.70 ± 0.37 | 0.76 ± 0.32 | 0.77 ± 0.32 |
| OCTMNIST | 0.67 ± 0.45 | 0.62 ± 0.48 | 0.63 ± 0.47 | 0.76 ± 0.37 | 0.64 ± 0.45 |
| PathMNIST | 0.69 ± 0.43 | 0.65 ± 0.47 | 0.61 ± 0.48 | 0.78 ± 0.36 | 0.70 ± 0.43 |
| Average | 0.74 ± 0.31 | 0.69 ± 0.37 | 0.71 ± 0.35 | 0.77 ± 0.31 | 0.76 ± 0.33 |

Table 7: Distribution of c values in $Trainable\ CT$, computed over all c parameters across all three runs of ImageNet-pretrained ResNet-18/50/152 and Imagenette-pretrained Swin-T/S when transferred to 12 downstream datasets. The three ResNet models exhibit similar distributions (means around 0.57–0.59, stds around 0.36–0.38), while the two Swin models also show comparable statistics with higher means (0.67–0.70), and similar stds (0.35-0.37). All models display substantial within-network variation, and the higher average c in Swin models may reflect insufficient pretraining relative to the ResNets.

| Dataset | ResNet-18 | ResNet-50 | ResNet-152 | Swin-T | Swin-S |
|-------------------|-----------------|-----------------|-----------------|-----------------|-----------------|
| Arabic Characters | 0.63 ± 0.39 | 0.61 ± 0.39 | 0.57 ± 0.37 | 0.66 ± 0.41 | 0.70 ± 0.38 |
| Arabic Digits | 0.59 ± 0.43 | 0.57 ± 0.42 | 0.55 ± 0.41 | 0.63 ± 0.45 | 0.71 ± 0.43 |
| Beans | 0.61 ± 0.29 | 0.54 ± 0.25 | 0.53 ± 0.23 | 0.67 ± 0.26 | 0.69 ± 0.24 |
| CUB-200 | 0.60 ± 0.37 | 0.63 ± 0.37 | 0.60 ± 0.34 | 0.70 ± 0.33 | 0.70 ± 0.33 |
| DTD | 0.59 ± 0.31 | 0.60 ± 0.32 | 0.57 ± 0.30 | 0.68 ± 0.25 | 0.74 ± 0.24 |
| FashionMNIST | 0.55 ± 0.44 | 0.60 ± 0.42 | 0.56 ± 0.42 | 0.62 ± 0.46 | 0.69 ± 0.43 |
| FGVC-Aircraft | 0.61 ± 0.36 | 0.63 ± 0.37 | 0.58 ± 0.35 | 0.71 ± 0.33 | 0.68 ± 0.33 |
| Flowers102 | 0.58 ± 0.26 | 0.54 ± 0.26 | 0.54 ± 0.23 | 0.65 ± 0.29 | 0.66 ± 0.25 |
| Food101 | 0.46 ± 0.47 | 0.63 ± 0.44 | 0.60 ± 0.43 | 0.72 ± 0.42 | 0.76 ± 0.39 |
| DermaMNIST | 0.58 ± 0.38 | 0.59 ± 0.37 | 0.57 ± 0.36 | 0.66 ± 0.36 | 0.71 ± 0.33 |
| OCTMNIST | 0.55 ± 0.45 | 0.60 ± 0.42 | 0.57 ± 0.42 | 0.58 ± 0.47 | 0.65 ± 0.45 |
| PathMNIST | 0.51 ± 0.45 | 0.58 ± 0.43 | 0.57 ± 0.42 | 0.71 ± 0.42 | 0.76 ± 0.40 |
| Average | 0.57 ± 0.38 | 0.59 ± 0.37 | 0.57 ± 0.36 | 0.67 ± 0.37 | 0.70 ± 0.35 |

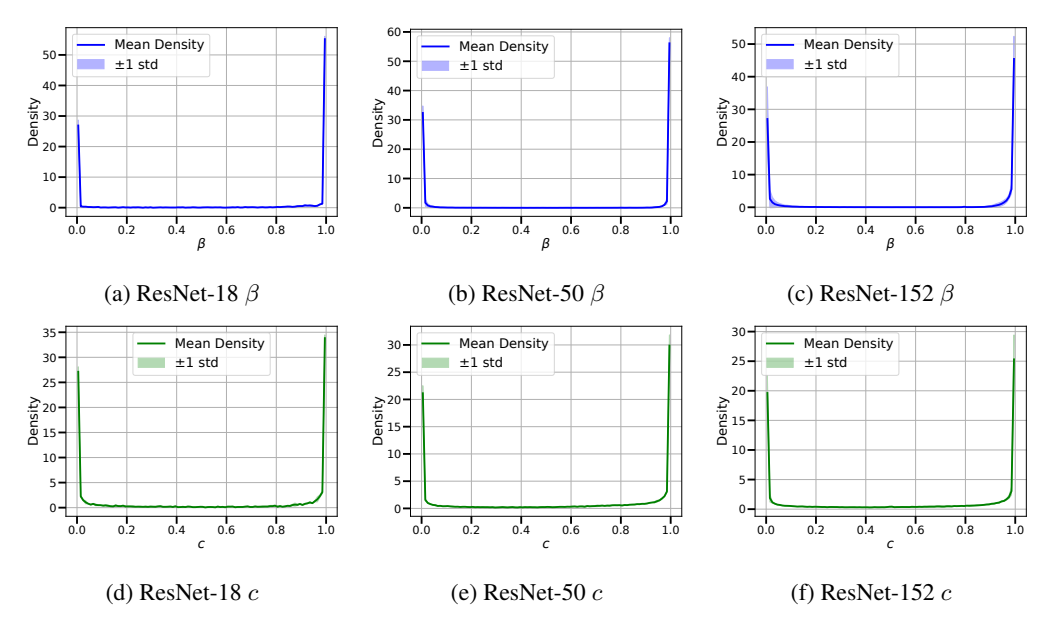


Figure 5: Common distributions of β (top) and c (bottom) in *Trainable CT* across ResNet-18/50/152, averaged over three runs (OCTMNIST shown as a representative dataset). Both β and c consistently exhibit sharp U-shaped distributions that appear similar across all models.

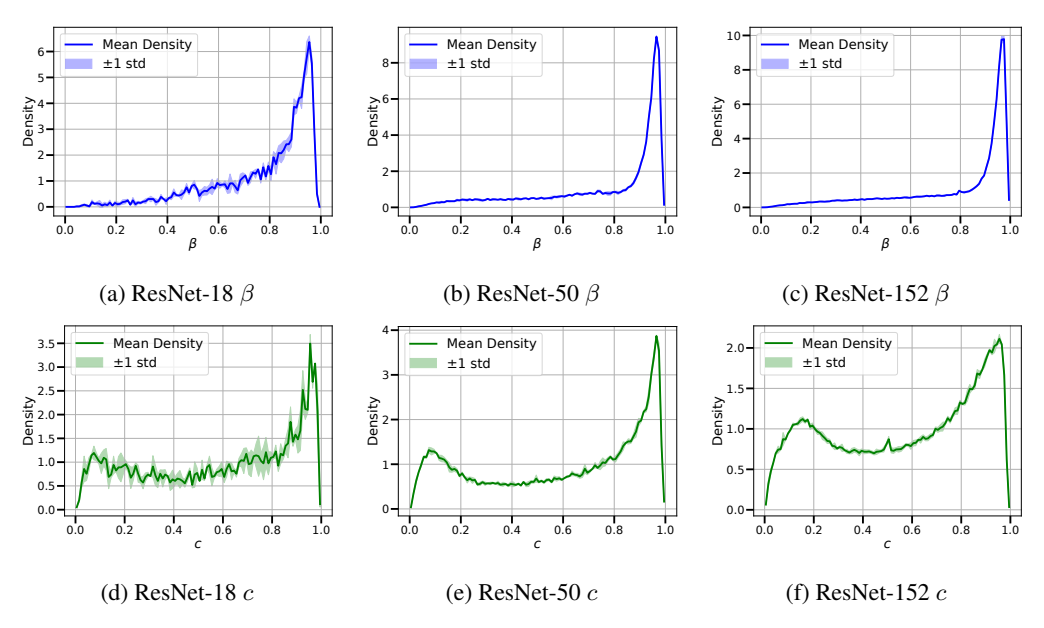


Figure 6: Uncommon distributions of β (top) and c (bottom) in *Trainable CT* across ResNet-18/50/152, averaged over three runs (DTD shown as an example dataset). While the overall shape is dataset-specific, the distributions of both β and c remain consistent across models.

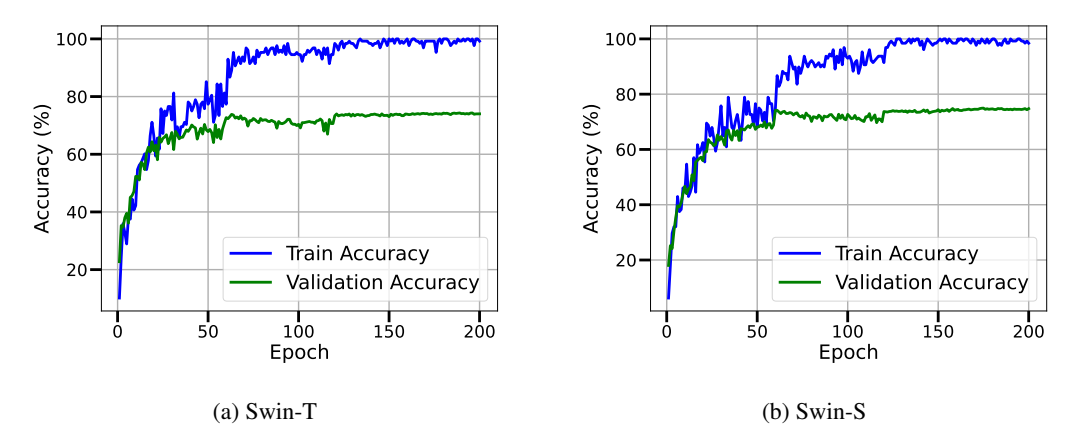


Figure 7: Training and validation accuracy curves for Swin-T and Swin-S during pretraining on Imagenette.

C Theoretical Intuition

This section provides theoretical intuition behind Curvature Tuning. Section C.1 casts CT as a projection over a space of smooth functions, while Section C.2 provides a toy example illustrating how CT can improve approximation of a target function of non-vanishing curvature, upon an ideal baseline ReLU network.

C.1 CT Operates as a Projection

At its core, Curvature Tuning operates by modulating the non-linearity of the activation functions of a trained model, providing a novel approach to model steering. In order to formalize the effect of CT, the following briefly introduces the notion of spaces of smooth functions.

Sobolev spaces Let $f: \mathbb{R}^d \to \mathbb{R}$ be a function and $\Omega \subseteq \mathbb{R}^d$ be a bounded domain. For $1 \leq p < \infty$, define $L^p(\Omega)$ as the space of functions $f: \Omega \to \mathbb{R}$ such that the L^p norm is finite, i.e.

$$||f||_{L^p(\Omega)} := \left(\int_{\Omega} |f(\mathbf{x})|^p d\mathbf{x}\right)^{\frac{1}{p}} < \infty$$
 (10)

Let $\alpha = (\alpha_1, \dots, \alpha_d)$ denote a multi-index, with $|\alpha| := \sum_i^d \alpha_i$, and $\alpha_i \in \mathbb{N}, \forall i = 1, \dots, d$. Let $q \in \mathbb{N}^*$. For $|\alpha| > 0$, define the Sobolev semi-norm

$$|f|_{W^{q,p}(\Omega)} := \left(\sum_{|\alpha| \le q} \|D^{\alpha} f\|_{L^p(\Omega)}^p\right)^{\frac{1}{p}} \tag{11}$$

with $D^{\alpha}f:=\frac{\partial^{|\alpha|}f}{\partial x_{1}^{\alpha_{1}}...\partial x_{d}^{\alpha_{d}}}$ denoting $|\alpha|$ -th order partial derivatives of f. Define the Sobolev norm

$$||f||_{W^{q,p}(\Omega)} := \left(||f||_{L^p(\Omega)}^p + |f|_{W^{q,p}(\Omega)}^p\right)^{\frac{1}{p}}$$
(12)

and the Sobolev space $W^{q,p}(\Omega):=\{f:\Omega\to\mathbb{R} \text{ s.t. } \|f\|_{L^p(\Omega)}^p+|f|_{W^{q,p}(\Omega)}^p<\infty\}.$

For a finite set $\mathcal{D} = \{\mathbf{x}_i\}_{i=1}^n$, the Sobolev semi-norm becomes

$$|f|_{W^{q,p}(\mathcal{D})} := \left(\sum_{|\alpha| \le q} \frac{1}{n} \sum_{i=1}^{n} \|D^{\alpha} f(\mathbf{x}_i)\|_p^p \right)^{\frac{1}{p}}$$
(13)

Finally, for $\mathbf{x} \in \mathbb{R}^d$, let $\|\mathbf{x}\|_p$ denote the p-norm, corresponding to the Euclidean norm for p = 2.

Curvature Tuning acts as a Sobolev Projection To characterize Curvature Tuning, we are interested in the space $W^{2,2}(\Omega)$, equipped with the Sobolev semi-norm

$$|f|_{W^{2,2}(\Omega)}^2 = \|\nabla_{\mathbf{x}}f\|_{L_2(\Omega)}^2 + \|\nabla_{\mathbf{x}}^2f\|_{L_2(\Omega)}^2$$
(14)

We begin by considering the Sobolev semi-norm of a ReLU network (equivalent to the case of Eq. (8) with $\beta \to 1$). For each $\mathbf{x} \in \mathbb{R}^d$, the gradient of a ReLU network

$$f(\mathbf{x}) = (W^L \circ \varphi \circ \dots \circ \varphi \circ W^1) (\mathbf{x})$$
(15)

with $\varphi(z) := \max(0, z)$, for $z \in \mathbb{R}$, is given by

$$\nabla_{\mathbf{x}} f(\mathbf{x}) = W^L \prod_{\ell=L-1}^{1} D^{\ell}(\mathbf{x}) W^{\ell}$$
(16)

where $D^{\ell}(\mathbf{x})$ is a diagonal matrix with $D^{\ell}_{ii}(\mathbf{x}) = \mathbf{1}_{\{\mathbf{z}^{\ell}_{i} > 0\}}$, with $\mathbf{z}^{\ell}_{i} = W^{\ell}_{i}\mathbf{z}^{\ell-1} + \mathbf{b}^{\ell}_{i}$ denoting the pre-activation of the ℓ -th layer, for $\ell = 1, \ldots, L$, with $\mathbf{z}^{0} := \mathbf{x}$.

We make the following observations:

- O1 Since ReLU networks are differentiable a. e., the gradients $\nabla_{\mathbf{x}} f(\mathbf{x})$ are bounded in norm by the network's Lipschitz constant, which can be defined as $C = \sup_{\mathbf{x} \in \Omega} \|\nabla_{\mathbf{x}} f(\mathbf{x})\|_2$. Hence, for $\Omega = \mathcal{D}$, the Lipschitz constant provides an upper bound on the first-order term of the Sobolev semi-norm in Equation 14.
- O2 Finally, we observe that since ReLU networks express piece-wise affine functions, the Hessian norm vanishes a.e. (i.e. wherever the Hessian is well defined), providing a bound on the second-order term of Equation 14.

Equipped with the above observations, in the following we characterize CT by formally restating and proving Theorem 3.1.

Theorem C.1. Let $f: \mathbb{R}^d \to \mathbb{R}$ denote a ReLU network, with model parameter W collecting all weights and biases. For $c \in [0,1]$ and fixed $\beta \in [0,1)$, replacing every instance of ReLU with a CTU (Equation 8) with hyperparameters β, c is equivalent to projecting f to a smooth function $f_{\beta,c} \in W^{2,2}(\Omega)$ in the Sobolev space $W^{2,2}(\Omega)$, with bounded Sobolev semi-norm.

Particularly, it holds $\|\nabla_{\mathbf{x}}^2 f(\mathbf{x})\|_{L^2(\Omega)} \leq \|\nabla_{\mathbf{x}}^2 f_{\beta,c}(\mathbf{x})\|_{L^2(\Omega)}$, from which $f_{\beta,a}$ enjoys higher local expressivity (non-vanishing curvature), while retaining the same model parameter \mathbf{W} .

Before proving Theorem C.1, we state the following Lemma, bounding the derivative of a CTU.

Lemma C.2. Let $\varphi_{\beta,c}(x)$ be defined according to Eq. (8), for $\beta \in [0,1)$ and $c \in [0,1]$. Then

$$\varphi'_{\beta,c}(x) = c\left(\sigma(bx) + bx\sigma(bx)(1 - \sigma(bx))\right) + (1 - c)\sigma\left(\frac{bx}{\beta}\right)$$
(17)

where $b := \frac{\beta}{1-\beta}$ and $\sigma(x) = \frac{\exp x}{1+\exp x}$ is the sigmoid activation.

Furthermore, $\exists \overline{h}_b \in \mathbb{R}^+$ *such that*

$$-c\overline{h}_b \le \varphi'_{\beta,c}(x) \le 1 + c\overline{h}_b \qquad \forall x \in \mathbb{R}, \quad \beta \in [0,1)$$
 (18)

Proof. We recall that, since $\forall x \in \mathbb{R}$, $\varphi_{\beta,c}(x)$ is defined as the convex combination of the SiLU activation function (c=1) and the SoftPlus activation (c=0), we can bound $\varphi'_{\beta,c}(x)$ by the convex combination of individual bounds obtained for the cases c=0 and c=1.

SoftPlus. If c=0, then $\varphi'_{\beta,0}(x)=\sigma\left(\frac{x}{1-\beta}\right)$ and $0\leq \varphi'_{\beta,0}(x)\leq 1\ \forall x$, since the derivative is defined as a sigmoid.

SiLU. If c=1, $\varphi'_{\beta,1}(x)=\sigma(bx)+bx\sigma(bx)(1-\sigma(bx))$. The first term in the sum is bounded by definition of sigmoid. For the second term, we note that $\sigma(bx)(1-\sigma(bx))$ is also bounded, and achieves it maximum at x=0, for which $0\leq\sigma(bx)(1-\sigma(bx))\leq\frac{1}{4}$. Furthermore, in the limit $x\to+\infty$, it holds $\varphi'_{\beta,1}(x)\to 1$, while $\varphi'_{\beta,1}(x)\to 0$ for $x\to-\infty$.

In the non-asymptotic regime, $\sigma(bx)(1-\sigma(bx))>0$, and so the maximum value of $bx\sigma(bx)(1-\sigma(bx))$ also depends on bx. To bound $\varphi'_{\beta,c}$ in this case, let us first consider x>0. By defining $\overline{h}_b=\max_{bx\geq 0}bx\sigma(bx)(1-\sigma(bx))$, then we finally obtain $0\leq \varphi'_{\beta,1}(x)\leq 1+\overline{h}_b$.

For the case x < 0, by using the identity $\sigma(x) = 1 - \sigma(-x)$, we have that $-\overline{h}_b \le \varphi'_{\beta,1}(x) \le 1$. By combining the results, we have

$$-\overline{h}_b \le \varphi'_{\beta,1}(x) \le 1 + \overline{h}_b \qquad \forall x \in \mathbb{R}, \quad \beta \in [0,1)$$
(19)

In conclusion, by convex combination of cases c=0 and c=1, Eq. (19) holds uniformly in x. \square

We can now prove Theorem C.1. To do so, for $f_{\beta,c}$ we have to show that

- 1. $f_{\beta,c}$ is smooth in \mathbf{x} , for $\mathbf{x} \in \Omega$
- 2. $||f_{\beta,c}||_{W^{2,2}(\Omega)} < \infty$

for a network $f_{\beta,c}$ obtained by replacing every ReLU φ with a CTU $\varphi_{\beta,c}$, while keeping all learned parameters **W** fixed.

Proof. We provide a proof for $\Omega = \mathcal{D} = \{\mathbf{x}_i\}_{i=1}^n$, under the common i.i.d. assumption on \mathcal{D} .

To prove the first point, we observe that for $\beta \in [0,1)$, the CTU activation function is smooth, i.e. $\varphi_{\beta,c} \in \mathcal{C}^{\infty}(\mathbb{R})$, thus making the whole network $f_{\beta,c}$ smooth.

We now consider the Sobolev semi-norm $|f_{\beta,c}|_{W^{2,2}(\Omega)}$. Starting with the first-order gradient, by recalling that CT replaces each occurrence of ReLU with the CTU activation function (Equation 8), the input gradient of CT is given by

$$\nabla_{\mathbf{x}} f_{\beta,c}(\mathbf{x}) = W^L \prod_{\ell=L-1}^{1} D_{\beta,c}^{\ell}(\mathbf{z}^{\ell}) W^{\ell}$$
(20)

where $D_{\beta,c}^{\ell}(\mathbf{z}^{\ell}) = \operatorname{diag}(\varphi_{\beta,c}^{\prime}(\mathbf{z}^{\ell}))$ with $\varphi_{\beta,c}^{\prime}(\mathbf{z}^{\ell})_i := \varphi_{\beta,c}^{\prime}(\mathbf{z}_i^{\ell})$ according to Eq. (17).

To bound the Jacobian norm, we observe that

$$\|\nabla_{\mathbf{x}} f_{\beta,c}(\mathbf{x})\| = \|W^L \prod_{\ell=L-1}^1 D_{\beta,c}^{\ell}(\mathbf{z}^{\ell}) W^{\ell}\|$$
(21)

$$\leq \|W^L\| \prod_{\ell=L-1}^1 \|D_{\beta,c}^{\ell}(\mathbf{z}^{\ell})\| \|W^{\ell}\| \tag{22}$$

$$\leq \|W^L\| \prod_{\ell=L-1}^1 \sqrt{d_\ell} (1 + c\overline{h}_b) \|W^\ell\| < \infty \qquad \text{(Lemma C.2)} \tag{23}$$

independent of x, for $W^{\ell} \in \mathbb{R}^{d_{\ell} \times d_{\ell-1}}$, with $d_0 := d$.

We now bound the second order term. By recalling that, for every $\mathbf{x} \in \mathbb{R}^d$, the Hessian $\mathbf{H}(\mathbf{x}) = \nabla_{\mathbf{x}}^2 f_{\beta,c}(\mathbf{x})$ is symmetric positive-definite, then for $\Omega = \mathcal{D}$ it holds

$$\|\nabla_{\mathbf{x}}^{2} f_{\beta,c}\|_{L_{2}(\mathcal{D})}^{2} = \frac{1}{n} \sum_{i=1}^{n} \|\mathbf{H}(\mathbf{x}_{i})\|_{2}^{2} \le \max_{1 \le i \le n} \lambda_{\max}^{2}(\mathbf{H}(\mathbf{x}_{i})) d_{\ell} < \infty$$
 (24)

with $\lambda_{\max}(\mathbf{H}(\mathbf{x}_i))$ denoting the largest singular value of $\mathbf{H}(\mathbf{x}_i)$.

Importantly, since a ReLU network f has vanishing curvature a.e., then for $0 \le \beta < 1$, we have

$$\|\nabla_{\mathbf{x}}^2 f(\mathbf{x})\| \leq \|\nabla_{\mathbf{x}}^2 f_{\beta,c}(\mathbf{x})\|.$$

Lastly, we note that, whenever Ω is a finite discrete set \mathcal{D} , $f_{\beta,c}$ is measurable, ensuring that $||f_{\beta,c}||_{W^{2,2}(\Omega)} < \infty$, concluding the proof.

Theorem C.1 shows that CT operates by projecting a ReLU network f to a smooth function $f_{\beta,c}$ in a restricted Sobolev space. Crucially, $f_{\beta,c}$ enjoys bounded gradients (and so is well behaved), and non-vanishing local-curvature for $0 < \beta < 1$, making it locally more expressive than the affine spline f, for fixed \mathbf{W} .

Furthermore, for fixed (β,c) , CT indeed operates as a projection, since replacing every ReLU with $\varphi_{\beta,c}$ is idempotent. Importantly, while for the original ReLU network $f \in W^{2,2}(\Omega)$ the derivatives $D^{\alpha}f$ are understood in a weak-sense, for $c \in [0,1]$ and $\beta \in [0,1)$, $f_{\beta,c}$ belongs to a Sobolev space $W^{2,2}_{\rm str}(\Omega) \subset W^{2,2}(\Omega)$ of smooth functions, whereby the derivative $D^{\alpha}f_{\beta,c}$ are understood in the strong (i.e. classical) sense.

We leave for future work extending our result to $Train\ CT$, which is associated with a non-convex optimization problem of finding optimal (β,c) for every neuron in the network. An additional important direction is to more closely compare $\|\nabla_{\mathbf{x}} f\|$ and $\|\nabla_{\mathbf{x}} f_{\beta,c}\|$, which may reveal more precise Lipschitz behaviour for CT, potentially better guiding the search for β and c.

C.2 Toy Example

We conclude the discussion by providing the full derivation for the motivating example in Section 3.

Consider a binary classification problem in \mathbb{R}^2 , whereby one is given two classes $\{\mathbf{x}\in\mathbb{R}^2:\|\mathbf{x}\|_2\leq\frac{1}{2}\}$ and $\{\mathbf{x}\in\mathbb{R}^2:\frac{3}{2}\leq\|\mathbf{x}\|_2\leq2\}$. The decision boundary maximizing the margin between the two classes is given by $S^1=\{\mathbf{x}\in\mathbb{R}^2:\|\mathbf{x}\|=1\}$.

For a ReLU network $f: \mathbb{R}^2 \to \mathbb{R}$, the maximum margin boundary is recovered by assigning $f(\mathbf{x}) = 0 \ \forall \mathbf{x} \in S^1$, for which $\sigma(f(\mathbf{x})) = 0.5$. To measure the approximation error e, the boundary is parameterized by $\gamma(t) = (\cos 2\pi t, \sin 2\pi t)$, for $t \in [0, 1]$.

Then, the error is expressed by the line integral $e = \int_{\gamma} |f| d\mathbf{x} = \int_{0}^{1} |f(\gamma(t))| \|\gamma'(t)\| dt$. Since f expresses an Affine Spline Operator, and each linear region in Ω is convex, then the integral along γ can be broken down into the integral along the intersection of γ with the spline partition Ω , i.e. $\Omega_{\gamma} := \Omega \cap S^{1}$. Importantly, this allows to pull back the affine spline breakpoints from Ω_{γ} to [0,1], so that $0 \le t_{1} \le \ldots \le t_{r'} = 1$, where $r' = |\Omega_{\gamma}|$. Then,

$$e = \int_0^1 |f(\gamma(t))| \|\gamma'(t)\| dt$$
 (25)

$$=2\pi \sum_{k=1}^{r'-1} \int_{t_k}^{t_{k+1}} |\mathbf{A}_{k,\cdot} \gamma(t) + \mathbf{b}_k| dt$$
 (26)

$$=2\pi \sum_{k=1}^{r'-1} \int_{t_k}^{t_{k+1}} (-1)^z \left(\mathbf{A}_{k,\cdot} \gamma(t) + \mathbf{b}_k\right) dt$$
 (27)

with $z := \mathbf{1}_{\{\mathbf{A}_{k,\cdot}\boldsymbol{\gamma}(t) + \mathbf{b}_{k} < 0\}}$. Then,

$$e = 2\pi \sum_{k=1}^{r'-1} \int_{t_k}^{t_{k+1}} (-1)^z \left(\mathbf{A}_{k,1} \cos 2\pi t + \mathbf{A}_{k,2} \sin 2\pi t + \mathbf{b}_k \right) dt$$
 (28)

$$=2\pi \sum_{k=1}^{r'-1} \int_{t_k}^{t_{k+1}} (-1)^z \left(\mathbf{A}_{k,1} \frac{\sin 2\pi}{2\pi} - \mathbf{A}_{k,2} \frac{\cos 2\pi}{2\pi} + \mathbf{b}_k t \right)_{t_k}^{t_{k+1}}$$
(29)

(30)

which evaluates to

$$e = \sum_{k=1}^{r'-1} (-1)^z \left(2\pi \mathbf{b}_k (t_{k+1} - t_k) + \mathbf{A}_{k,1} \left(2\sin\frac{t_{k+1} - t_k}{2}\cos\frac{t_{k+1} - t_k}{2} - \mathbf{A}_{k,2} \left(2\sin\frac{t_{k+1} + t_k}{2}\sin\frac{t_k - t_{k+1}}{2} \right) \right)$$
(31)

from which clearly $e \to 0 \iff t_{k+1} \to t_k \quad \forall k$.

Hence, assuming the ReLU network considered attained optimal approximation error e>0, reducing the error further requires increasing the number of breakpoints of the ASO, in turn requiring a degree of retraining (either through PEFT or training from scratch). With this view, Curvature Tuning opens an additional avenue for model adaptation: steering the model's decision boundaries by modulating the non-linearity of the activation function, allowing to tune a model towards optimality without expensive retraining. To this end, it is important to note that modulating decision boundaries is orthogonal to feature adaptation and finetuning, since it allows to change the shape of decision boundaries while keeping the model parameter ${\bf W}$ fixed.

D Curvature Tuning (CT) implementation

The following code provides the Python implementation for CT and Trainable CT:

- CTU & TrainableCTU: classes that define the CTU module used in CT and Trainable CT, respectively.
- replace_module & replace_module_dynamic: functions that apply the appropriate module replacement to integrate *CT* or *Trainable CT* into a model.

```
import torch
from torch import nn
import torch.nn.functional as F
class CTU(nn.Module):
   CTU for CT.
   def __init__(self, shared_raw_beta, shared_raw_coeff, threshold
        super().__init__()
        self.threshold = threshold
        self._raw_beta = shared_raw_beta
        self._raw_coeff = shared_raw_coeff
        self._raw_beta.requires_grad = False
        self._raw_coeff.requires_grad = False
    @property
    def beta(self):
        return torch.sigmoid(self._raw_beta)
    @property
    def coeff(self):
        return torch.sigmoid(self._raw_coeff)
    def forward(self, x):
        beta = torch.sigmoid(self._raw_beta)
        coeff = torch.sigmoid(self._raw_coeff)
        one_minus_beta = 1 - beta + 1e-6
        x_scaled = x / one_minus_beta
        return (coeff * torch.sigmoid(beta * x_scaled) * x +
                (1 - coeff) * F.softplus(x_scaled, threshold=self.
                threshold) * one_minus_beta)
```

```
class TrainableCTU(nn.Module):
    """
    CTU for Trainable CT.
    """

def __init__(self, num_input_dims, out_channels, raw_beta=1.386,
    raw_coeff=0.0, threshold=20):
        super().__init__()
        self.threshold = threshold

# Decide channel dim based on input shape
    if num_input_dims == 2 or num_input_dims == 3: # (B, C) or (B, L, D)
        channel_dim = -1
    elif num_input_dims == 4: # (B, C, H, W)
        channel_dim = 1
    else:
        raise NotImplementedError(f"Unsupported input dimension {
        num_input_dims}")
```

```
param_shape = [1] * num_input_dims
    param_shape[channel_dim] = out_channels
    # Init beta
    self._raw_beta = nn.Parameter(torch.full(param_shape, float(
   raw_beta)))
    # Init coeff
    self._raw_coeff = nn.Parameter(torch.full(param_shape, float(
    raw_coeff)))
@property
def beta(self):
    return torch.sigmoid(self._raw_beta)
@property
def coeff(self):
    return torch.sigmoid(self._raw_coeff)
def forward(self, x):
   beta = torch.sigmoid(self._raw_beta)
    coeff = torch.sigmoid(self._raw_coeff)
    one_minus_beta = 1 - beta + 1e-63
   x_scaled = x / one_minus_beta
   return (coeff * torch.sigmoid(beta * x_scaled) * x +
            (1 - coeff) * F.softplus(x_scaled, threshold=self.
            threshold) * one_minus_beta)
```

```
def replace_module(model, old_module=nn.ReLU, new_module=CTU, **kwargs
    Replace all instances of old_module in the model with new_module.
    device = next(model.parameters(), torch.tensor([])).device #
   Handle models with no parameters
    # Replace modules
   for name, module in model.named_modules():
        if isinstance(module, old_module):
            ct = new_module(**kwargs).to(device)
            # Replace module in the model
            names = name.split(".")
            parent = model
            for n in names[:-1]:
                if n.isdigit():
                    parent = parent[int(n)] # for Sequential/
                    ModuleList
                else:
                    parent = getattr(parent, n)
            last_name = names[-1]
            if last_name.isdigit():
                parent[int(last_name)] = ct # for Sequential/
                ModuleList
                setattr(parent, last_name, ct)
   return model
```

```
def replace_module_dynamic(model, input_shape, old_module=nn.ReLU,
new_module=TrainableCTU, **kwargs):
```

```
Replace all instances of old_module in the model with new_module
that's dynamically created based on the number of output channels.
device = next(model.parameters(), torch.tensor([])).device
dummy_input = torch.randn(*input_shape).to(device)
module_metadata = {} # name -> (num_input_dims, out_channels)
hooks = []
def make_hook(name):
    def hook(module, input, output):
        num_input_dims = input[0].dim()
        if num_input_dims in (2, 3):
                                        # (B, C) or (B, L, D)
            out_channels = output.shape[-1]
        elif num_input_dims == 4:
                                         # (B, C, H, W)
            out_channels = output.shape[1]
            raise NotImplementedError(f"Unsupported output shape {
            output.shape} in {name}")
        module_metadata[name] = (num_input_dims, out_channels)
    return hook
# Register hooks to all modules of the target type
for name, module in model.named_modules():
    if isinstance(module, old_module):
        hooks.append(module.register_forward_hook(make_hook(name))
# Run dummy forward pass
model(dummy_input)
# Clean up hooks
for hook in hooks:
    hook.remove()
# Replace modules
for name, module in model.named_modules():
    if isinstance(module, old_module) and name in module_metadata:
        num_input_dims, out_channels = module_metadata[name]
        ct = new_module(num_input_dims=num_input_dims,
        out_channels=out_channels, **kwargs).to(device)
        # Replace module in the model
        names = name.split(".")
        parent = model
        for n in names[:-1]:
            if n.isdigit():
                parent = parent[int(n)] # for Sequential/
                ModuleList
            else:
                parent = getattr(parent, n)
        last_name = names[-1]
        if last_name.isdigit():
            parent[int(last_name)] = ct # for Sequential/
            ModuleList
        else:
            setattr(parent, last_name, ct)
return model
```

E LoRA Implementation

The following code provides the Python implementation of LoRA used in Section 4:

- LoRALinear & LoRAConv2d: classes that define LoRA-enhanced versions of the Linear and Conv2d modules.
- get_lora_model: a function that replaces all Linear and Conv2d modules in a model with their corresponding LoRA versions.

```
import torch
from torch import nn as nn
from torch.nn import functional as F
class LoRALinear(nn.Module):
   A Linear layer that applies LoRA to a frozen, pretrained Linear.
    def __init__(self, original_layer: nn.Linear, r: int = 4, alpha:
    float = 1.0):
        super().__init__()
        self.in_features = original_layer.in_features
        self.out_features = original_layer.out_features
        self.r = r
        self.alpha = alpha
        # Freeze the original layer's parameters
        self.weight = nn.Parameter(original_layer.weight.data,
        requires_grad=False)
        if original_layer.bias is not None:
            self.bias = nn.Parameter(original_layer.bias.data,
            requires_grad=False)
        else:
            self.bias = None
        # LoRA parameters B and A
        # B: [out_features, r]
        # A: [r, in_features]
        self.B = nn.Parameter(torch.zeros((self.out_features, r)))
        self.A = nn.Parameter(torch.zeros((r, self.in_features)))
        # Initialize LoRA weights
        nn.init.kaiming_uniform_(self.B, a=5 ** 0.5)
        nn.init.zeros_(self.A)
    def forward(self, x):
        # Normal forward with the frozen weight
        result = F.linear(x, self.weight, self.bias)
        # LoRA path: B @ A
        # shape of BA = [out_features, in_features]
        # Then F.linear with BA
        lora_update = F.linear(x, (self.alpha / self.r) * (self.B @
        self.A))
        return result + lora_update
```

```
class LoRAConv2d(nn.Module):
    """
    A Conv2d layer that applies LoRA to a frozen, pretrained Conv2d.
    """
```

```
def __init__(self, original_layer: nn.Conv2d, r: int = 4, alpha:
float = 1.0):
    super().__init__()
    self.out_channels = original_layer.out_channels
    self.in_channels = original_layer.in_channels
    self.kernel_size = original_layer.kernel_size
    self.stride = original_layer.stride
    self.padding = original_layer.padding
    self.dilation = original_layer.dilation
    self.groups = original_layer.groups
    self.bias_available = (original_layer.bias is not None)
    self.r = r
    self.alpha = alpha
    # Freeze original parameters
    self.weight = nn.Parameter(original_layer.weight.data,
    requires_grad=False)
    if self.bias_available:
        self.bias = nn.Parameter(original_layer.bias.data,
        requires_grad=False)
        self.bias = None
    # Flattened shape for weight is [out_channels, in_channels *
    k_h * k_w]
    k_h, k_w = self.kernel_size
   fan_in = self.in_channels * k_h * k_w # Flattened input dim
    # Define LoRA parameters: B and A
    # B: [out_channels, r]
   # A: [r, fan_in]
    self.B = nn.Parameter(torch.zeros((self.out_channels, r)))
   self.A = nn.Parameter(torch.zeros((r, fan_in)))
   # Initialize LoRA weights
   nn.init.kaiming_uniform_(self.B, a=5 ** 0.5)
   nn.init.zeros_(self.A)
def forward(self, x):
    # Standard (frozen) convolution
   result = F.conv2d(
        х,
        self.weight,
        bias=self.bias,
        stride=self.stride,
        padding=self.padding,
        dilation=self.dilation,
        groups=self.groups
   )
   # Compute LoRA update
    # 1) Flatten conv kernel in the same manner as above
   # 2) Multiply B and A -> shape [out_channels, in_channels *
   k_h * k_w]
    # 3) Reshape it back to [out_channels, in_channels, k_h, k_w]
   BA = self.B @ self.A # shape [out_channels, fan_in]
    # Reshape to conv kernel
   k_h, k_w = self.kernel_size
   lora_weight = BA.view(
        self.out_channels,
        self.in_channels,
        k_h,
```

```
def get_lora_model(model: nn.Module, r: int = 4, alpha: float = 1.0):
   Recursively replace all Conv2d and Linear modules in model with
   LoRA-enabled versions. Freezes original weights and adds LoRA
   parameters.
    11 11 11
   for name, child in list(model.named_children()):
        # If child is a Conv2d, replace it with LoRAConv2d
        if isinstance(child, nn.Conv2d):
            lora_module = LoRAConv2d(child, r=r, alpha=alpha)
            setattr(model, name, lora_module)
        # If child is a Linear, replace it with LoRALinear
        elif isinstance(child, nn.Linear):
            lora_module = LoRALinear(child, r=r, alpha=alpha)
            setattr(model, name, lora_module)
        else:
            # Recursively traverse children
            get_lora_model(child, r=r, alpha=alpha)
    return model
```